

# Characteristics of the Large-Area Stacked Microstructured Semiconductor Neutron Detector

S.L. Bellinger<sup>\*a</sup>, R.G. Fronk<sup>a</sup>, T.J. Sobering<sup>b</sup>, D.S. McGregor<sup>a</sup>

<sup>a</sup>S.M.A.R.T. Laboratory, Department of Mechanical and Nuclear Engineering,  
Kansas State University, Manhattan, KS 66506

<sup>b</sup>Electronics Design Laboratory,  
Kansas State University, Manhattan, KS 66506

## ABSTRACT

Silicon diodes with large aspect ratio microstructures backfilled with  ${}^6\text{LiF}$  show a dramatic increase in neutron detection efficiency beyond that of conventional thin-film coated planar devices. Described in this work are advancements in the technology with increased microstructure depths and detector stacking methods that work to increase thermal-neutron detection efficiency. An individual  $4\text{-cm}^2$  MSND was fabricated. A stacked  $4\text{-cm}^2$  MSND was fabricated by coupling two detectors back-to-back, along with counting electronics, into a single detector. The individual MSND delivered 16% intrinsic thermal-neutron detection efficiency and the stacked MSND delivered 32% intrinsic thermal-neutron detection efficiency. The intrinsic thermal-neutron detection efficiency depends strongly upon the geometry, size, and depth of the silicon microstructures. This work is part of on-going research to develop solid-state semiconductor neutron detectors with high neutron detection efficiencies.

**Keywords:** solid state neutron detectors, perforated detectors, microstructured semiconductor diode, He-3 replacement technology

## 1. INTRODUCTION

Microstructured semiconductor neutron detectors (MSNDs) are fabricated by etching microstructured patterns into a semiconductor diode and then backfilling these microstructures with a neutron conversion material such as  ${}^{10}\text{B}$  or  ${}^6\text{LiF}$ . The energetic charged-particle reaction products can be captured within the semiconductor diode, thereby, recording a neutron interaction. The deep microstructures, backfilled with neutron reactive material, increase the neutron absorption efficiency by increasing the probability of registering an interaction.

Inductively-coupled-plasma reactive-ion-etching (ICP-RIE) using high-aspect ratio deep etching (HARDE) techniques, along with common MEMS wet-etching techniques [1], are used to fabricate the etched features. MSNDs etched with a straight-trench microstructure pattern (200 microns in depth), each with a  $4\text{-cm}^2$  active-area, have been fabricated and backfilled with  ${}^6\text{LiF}$  neutron absorber material. Individual and stacked MSNDs have been assembled and tested for intrinsic neutron detection efficiency and gamma-ray sensitivity. The detectors were operated with amplifiers designed by the Kansas State University (KSU) Electronics Design Laboratory (EDL).

### 1.1 State of the art

Although the microstructured neutron detector achieves high thermal-neutron detection efficiency with a single device, designs in which two detectors are stacked, in a staggered fashion, offer the best performance and highest efficiencies. Models of the straight trench detector design, in a stacked configuration, were developed in [2] to determine the optimum design parameters to achieve the best efficiency while preserving a high  $n/\gamma$  discrimination ratio. A large-area stacked device, in which two MSNDs were connected back-to-back into a single detector, was fabricated to demonstrate and test the principle. The intrinsic thermal-neutron detection efficiency for normal incident  $0.0253\text{ eV}$  neutrons was measured against a calibrated  ${}^3\text{He}$  proportional counter.

## 2. DETECTOR DESIGN

### 2.1 Basic stacked MSND design and model geometry

The design studied in the present work consisted of MSNDs with straight parallel trenches backfilled with  ${}^6\text{LiF}$  ( ${}^6\text{Li}$  isotopically purified >95%). A detailed discussion on the selection of substrate materials and neutron reactive materials is presented elsewhere [2, 3]. Shown in Fig. 1 is the basic stacking concept for the MSNDs, in which a second detector is offset from the first detector to reduce neutron streaming through the structure. Note that the 2200 m/s neutron absorption cross section of silicon is small,  $\sigma_{\text{Si,a}} = 0.171 \text{ b}$  [4], indicating that the Si substrate does not appreciably attenuate neutrons passing through the substrate of the first detector and into the second detector.

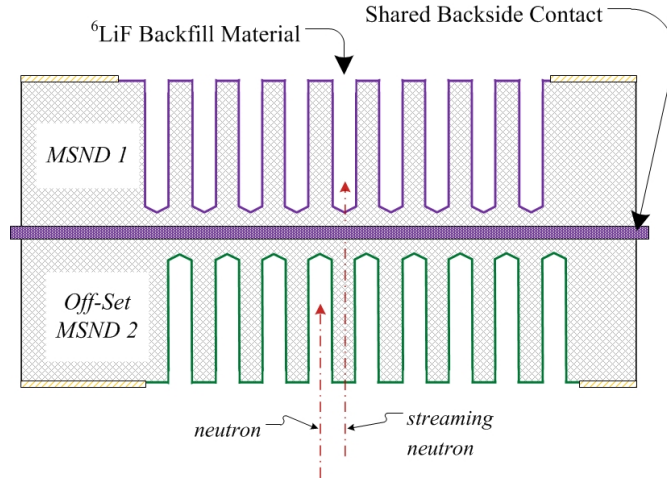


**Fig. 1.** The “trench design,” composed of etched grooves backfilled with neutron reactive material, showing that neutron detection efficiency is increased, and streaming minimized, by stacking a 2<sup>nd</sup> detector off-set from the first.

Neutrons that stream orthogonally through the silicon detection material and are not captured, may be caught by a second properly arranged off-set detector from the first detector. Some microstructure patterns are better suited for this stacking arrangement than others. For instance, double stacking of the cylindrical-hole, cylindrical columns, or hexagonal-hole microstructure patterns do not offer a solution to completely blocking the path of a normally incident parallel beam of neutrons, as discussed elsewhere [2]. A stacked straight trench microstructure pattern can be designed to eliminate neutron streaming through the stacked MSNDs (see Fig. 1).

### 2.2 Discussion

The neutron detection efficiency of the compact MSNDs can be greatly improved by stacking two offset devices and operating them as a single unit detector. Of the microstructure geometries presented elsewhere [2, 3, 5, 6], only the trench design and its variants can be stacked such that the front device converter does not shadow the second device converter, while still allowing for the sum of the converter areas to completely fill the total detector area. In other words, the efficiency can be doubled for a trench-style device and variants while eliminating neutron streaming paths, features not possible with other etched patterns. The optimum case for stacked straight trench devices requires that the features be symmetric (trench and semiconductor fin widths are equal). However, if the detector is to be operated as a single device, an asymmetric design, where more neutron converter material is present, may yield higher efficiencies [3].

There are non-ideal conditions that will reduce the calculated efficiencies presented in previous MSND simulation work [1-3]. These conditions include incomplete charge collection, long carrier-transport times in the semiconductor that cause ballistic deficit, and leakage currents that increase system noise. Additionally, inactive regions near the etched surface of the semiconductor, caused by mechanical or chemical damage, will absorb reaction product energy before they reach the semiconductor active region. Collectively, these effects contribute to a spectral shift and ultimately a lower measured neutron detection efficiency than predicted by theory.

### 3. STACKED MSND FABRICATION AND TESTING

#### 3.1 Fabrication Methodology of the 4-cm<sup>2</sup> MSND

The detectors were batch-processed on 3-inch diameter high-resistivity 10 k $\Omega$ -cm *n*-type Si wafers. A thick wet oxide was initially grown, through which a diffusion window was lithographically patterned. Microstructured straight trenches were then etched into the Si diffusion windows with an ICP-RIE process [7]. Individual detectors were designed with 4-cm<sup>2</sup> active areas. The individual devices had straight trenches etched 200 microns deep by 30 microns wide with a center line pitch of 60 microns. The straight trench design maintains high neutron detection efficiency while creating an opportunity to off-set and stack the detector chips to maximize neutron absorption (as shown in Fig. 1). After the etch process, the wafer was chemically cleaned and *p*-type regions were diffused uniformly into individual device microstructures across the wafer, thereby forming *pn* junctions within the trenches. A Ti-Au metal contact was fabricated on the backside of the wafer to make an electrical ground contact, thereby, completing the diode structure and enabling depletion through the bulk of the individual devices. Finally, <sup>6</sup>LiF powder was packed into the microstructures to function as the neutron absorbing converter material (see Fig. 2 for illustration).

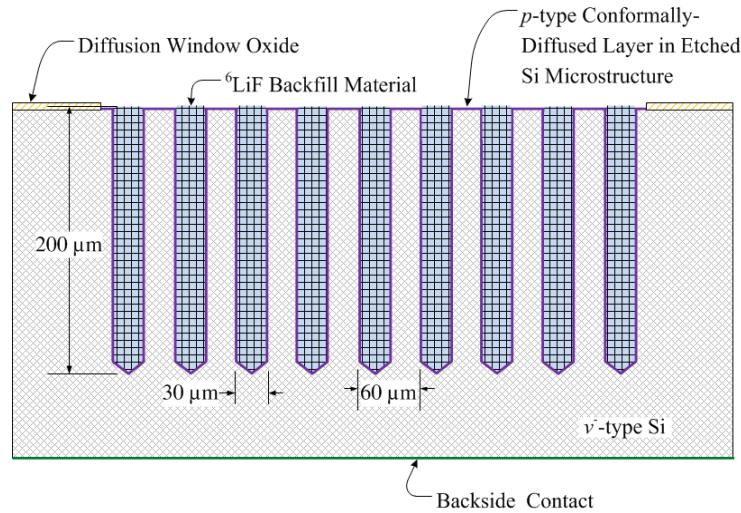


**Fig. 2.** Cross-section illustration of a fabricated MSND with conformally-diffused diode structure.

Large-area 4-cm<sup>2</sup> individual and stacked MSNDs were mounted in two identical detector systems. The individual and stacked detector amplifying and readout electronics were designed in-house by EDL and consist of a sandwiched detector board and a separate motherboard (see Fig. 3). The separate motherboard configuration was used for research purposes, an arrangement that simplifies the testing of multiple detector types through the use of common electronics. On the preamplifier board, a copper foil is sandwiched between the two printed circuit boards that have an exposed backside plane. The copper foil provides electrical connection for the positive bias voltage to the MSNDs. An individual MSND and two MSNDs mounted back-to-back were bonded to the copper foil of the preamplifier using conductive silver epoxy. The MSND's anodes were wire-bonded to gold pads that are electrically connected by a post through the sandwiched boards on the preamplifier. In the configuration for the stacked MSNDs, the anodes of each detector are common and applied to the input of the charge sensitive preamplifier. A relatively short time constant is used because high counting rates are expected for some applications. The preamplifier board can also be reconfigured such that the feedback from a downstream integrator can be applied to compensate for the large leakage currents that may result from the detector processing steps (see Fig. 4 for circuit diagram). All connections to and from the preamplifier board were on a single row 10-pin edge connector. Because the detectors are photosensitive, the individual MSND and stacked MSNDs, along with the motherboard, were placed in a shielded aluminum box.

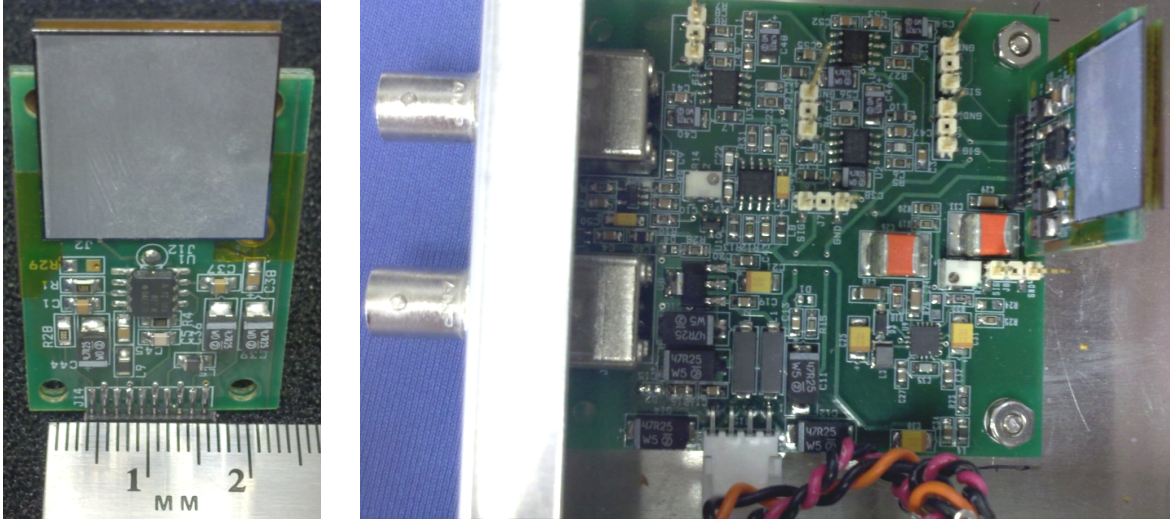


**Fig. 3.** Shown are (left) the 4-cm<sup>2</sup>, large-area, dual-integrated, stacked, MSND package with preamplifying circuitry and (right) a picture of the detector package and motherboard. The motherboard provides an adjustable detector bias, bias-current compensation, pulse shaping and gain, an analog output for pulse-height analysis, and a digital output from a discriminator.

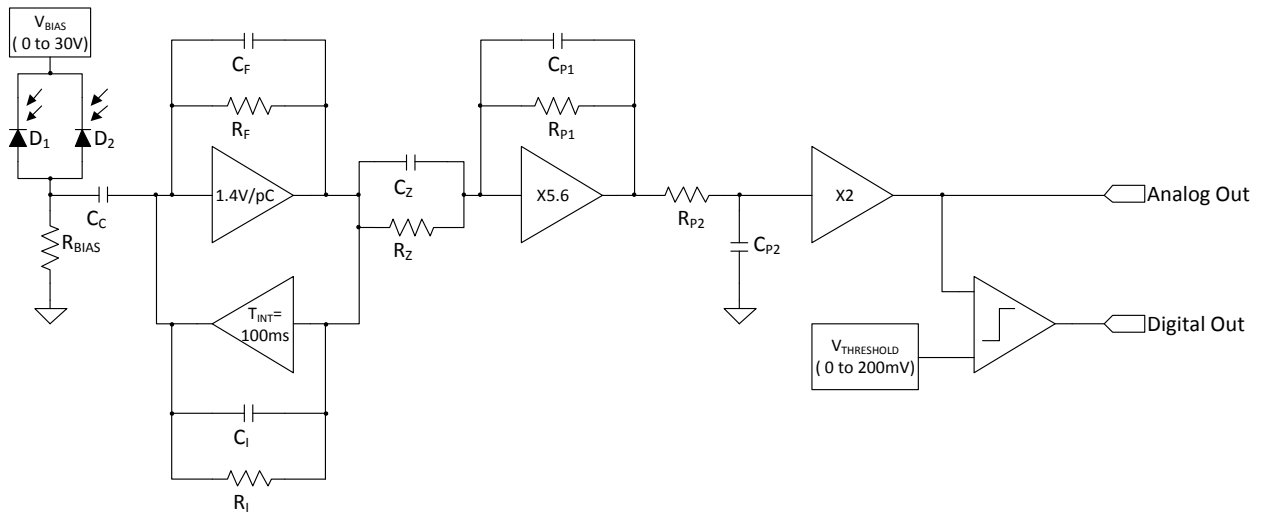


**Fig. 4.** Diagram of the 4-cm<sup>2</sup> dual-integrated stacked MSND's basic readout circuit for pulse amplification, adjustable detector bias, bias current compensation, pulse shaping and gain, analog output for pulse-height analysis, and digital output from a discriminator.

### 3.2 Performance of Large-Area Individual and Stacked 4-cm<sup>2</sup> MSNDs

The stacked-detector thermal-neutron counting efficiency was measured with a 0.0253 eV diffracted neutron beam from the Kansas State University TRIGA Mark II nuclear reactor. The neutron flux was calibrated with a Reuter-Stokes <sup>3</sup>He gas-filled proportional detector and found to be  $1.05 \pm 0.02 \times 10^4 \text{ cm}^{-2} \text{ s}^{-1}$ . Details of the calibration method can be found elsewhere [8, 9]. In addition, by using a diffracted thermal-neutron beam, a direct comparison can be made between the experimental performance of the MSNDs and that of the modeled thermal-neutron detection efficiencies and ion energy-deposition spectra reported elsewhere [2, 3]. A pulse-height spectrum was collected from the individual and stacked MSNDs in the diffracted neutron beam with and without a beam blocking Cd-shutter so as to allow the collection of neutron responses with and without thermal-neutrons. Prompt gamma-rays emitted from the thin Cd-shutter appear in the spectrum as numerous pulses at low energy near the noise floor of the detector system (see Fig. 5).

In addition, because the measurement was performed near a nuclear reactor, there is an appreciable albedo neutron background observed as counts above channel 25 in the background measurement (see Figs. 4 and 5). For pulse height spectra collected from either individual MSND or the stacked MSNDs (with an lower level discriminator (LLD) set above the system electronic noise), the neutron counting efficiency was calculated by dividing the summed neutron counts by the calibrated neutron flux determined with the  $^3\text{He}$  detector.

A pulse-height spectrum was collected from an individual 4-cm<sup>2</sup> MSND with a 10- $\mu\text{s}$  charge integration time in the diffracted neutron beam with and without a beam blocking Cd-shutter so as to allow the collection of responses with and without thermal-neutrons (see Fig. 5). Additionally, because the diffracted neutron beam is not composed purely of thermal neutrons [10], it is possible that some epi-thermal and fast neutrons, not absorbed in the Cd-shutter, are measured by the MSND. The 4-cm<sup>2</sup> MSND operated on 1 volt of reverse bias. Notice in Fig. 5 that the pulse-height spectrum is significantly separated from the noise/gamma-ray floor. Although the single MSND is 2 times larger than previously stacked 1-cm<sup>2</sup> MSNDs [11], the charge collection is still complete and, thus, forms large distinguishable neutron interaction pulses. In addition, the MSND exhibits the expected spectral shape predicted elsewhere [3], with a pulse-height frequency dip at low energy.

For the 4-cm<sup>2</sup> large-area MSND design, with the LLD set to channel 25 (slightly above the majority of the background counts), the intrinsic thermal-neutron detection efficiency was measured to be  $16.33 \pm 0.09\%$ . For the MSND design, with the LLD set to channel 32, the intrinsic thermal-neutron detection efficiency was measured to be  $15.94 \pm 0.09\%$ . Notice that by increasing the LLD from channel 25 to 32, the thermal-neutron detection efficiency only decreased by 0.39% in efficiency. This dip in the pulse height spectrum in the low-energy region is vitally important for retaining neutron detection efficiency while effectively discriminating background radiation.

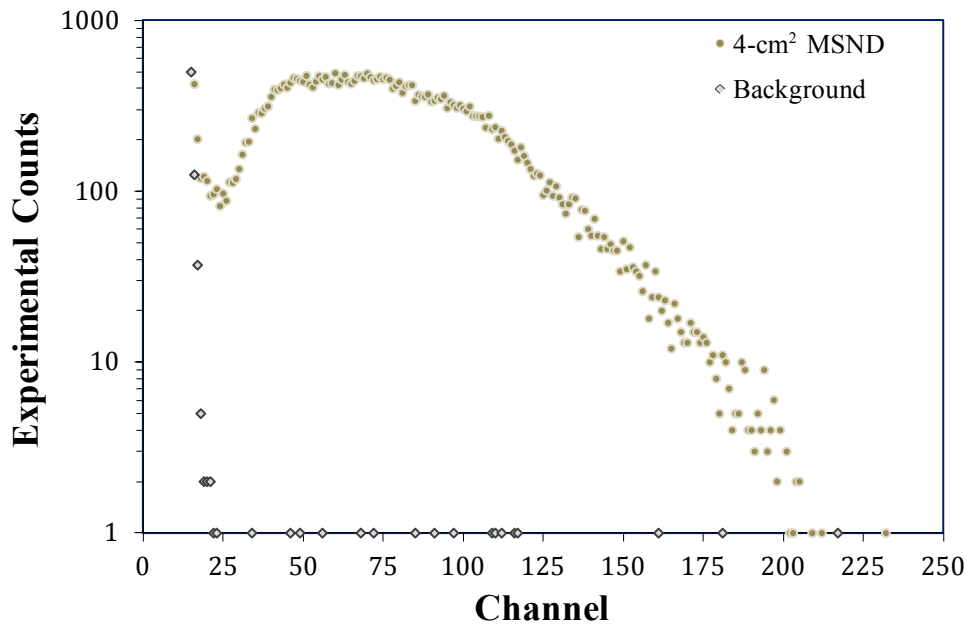


**Fig. 5.** Pulse-height spectrum for an individual 4-cm<sup>2</sup> MSND with 200- $\mu\text{m}$  deep, straight trench microstructures backfilled with  $^6\text{LiF}$ . At an LLD = 25 Chn, the measured intrinsic thermal-neutron detection efficiency was 16.3%, and at an LLD = 32 Chn the measured thermal-neutron detection was 15.9%.

To further improve neutron detection efficiency, individual large-area 4-cm<sup>2</sup> MSND chips were stacked back-to-back, as was configured with early generation 1-cm<sup>2</sup> MSNDs [11]. Dual-integrated neutron counting efficiency was measured for a stacked MSND configuration of two 200- $\mu\text{m}$  deep, 4-cm<sup>2</sup> area, MSNDs. The stacked dual-integrated MSNDs operated with 1 volt of reverse bias. The combined leakage current for the 4-cm<sup>2</sup> stacked MSNDs was 78 nA. A pulse-height spectrum from a dual-integrated stacked 4-cm<sup>2</sup> MSND is shown in Fig. 6. Notice in Fig. 6 that the pulse-height spectrum of the dual integrated detector shows a downward shift of the pulse-height signal compared to an

individual 4-cm<sup>2</sup> MSND. Some of this shift may be because of an overall increase in capacitance of the stacked MSNDs, thereby reducing the pulse-height signal from the detector. For the stacked large-area 4-cm<sup>2</sup> MSND design, with the LLD set to channel 18, just above the majority of the background signal, the intrinsic efficiency was measured to be  $32.39 \pm 0.16\%$ . With the LLD raised to channel 28, the intrinsic efficiency was measured to be  $28.99 \pm 0.14\%$ .

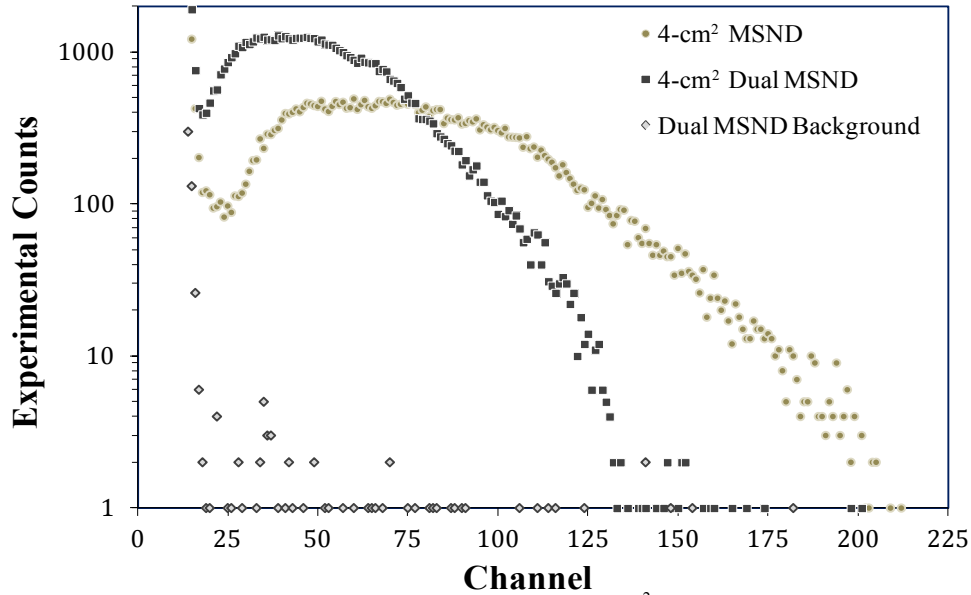


**Fig. 6.** Comparison of pulse-height spectra from the individual and stacked 4-cm<sup>2</sup> MSNDs, each with 200- $\mu$ m deep, straight trench microstructures backfilled with <sup>6</sup>LiF. For the stacked MSND, at an LLD = 18 Chn, the measured thermal-neutron detection efficiency was 32.4%, and at an LLD = 28 Chn the measured thermal-neutron detection efficiency was 29.0%.

### 3.3 Gamma-Ray Discrimination for the Large-Area 4-cm<sup>2</sup> MSNDs

The individual and stacked 4-cm<sup>2</sup> large-area MSNDs were independently tested with a <sup>137</sup>Cs source with an activity of 71.69 mCi, to determine the gamma-ray detection efficiency, i.e., rejection ratio. The gamma-ray source was placed 50 cm away from the detector and a counting spectrum was taken. A background count was also taken to subtract any background counts and noise contributions. The gamma-ray rejection ratio was determined by dividing the integrated gamma-ray counts in the measured spectrum by the source gamma-ray fluence passing through the 4-cm<sup>2</sup> MSND (adjusted by detector fractional solid angle  $\Omega_F$  [9]). The gamma-ray pulse-height spectrum response is shown in Fig. 7.

With the LLD set at channel 25, the gamma-ray detection efficiency was determined to be approximately  $1.85 \times 10^{-6}$  measured-event per gamma ray, and with the LLD set to channel 32 the gamma-ray detection efficiency is approximately  $3.95 \times 10^{-8}$  measured-event per gamma ray. The neutron to gamma-ray rejection ratio ( $n/\gamma$ ) for 662 keV photons is then easily calculated by dividing the MSND detection efficiency by the gamma-ray detection efficiency. The  $n/\gamma$  ratio for the stacked MSND with an LLD set at channel 25 is  $8.83 \times 10^4$ , and with an LLD set at channel 32 the  $n/\gamma$  ratio is  $4.04 \times 10^6$ . These data are summarized in Table 1. Similar to the stacked 1-cm<sup>2</sup> MSND reported elsewhere [11], the deeper microstructured trench shows that the gamma-ray interaction pulse heights from the MSND are small, resulting in superior gamma-ray discrimination. Also, the individual 4-cm<sup>2</sup> MSND has more bulk silicon with which gamma rays can interact than the 1-cm<sup>2</sup> detectors, yet the  $n/\gamma$  is better for the 4-cm<sup>2</sup> MSND because of higher frequency of larger pulse heights from neutron interactions. Again, the MSND gamma-ray response measurement was performed in the KSU reactor bay, which has a higher background of albedo neutrons than natural neutron background [12].

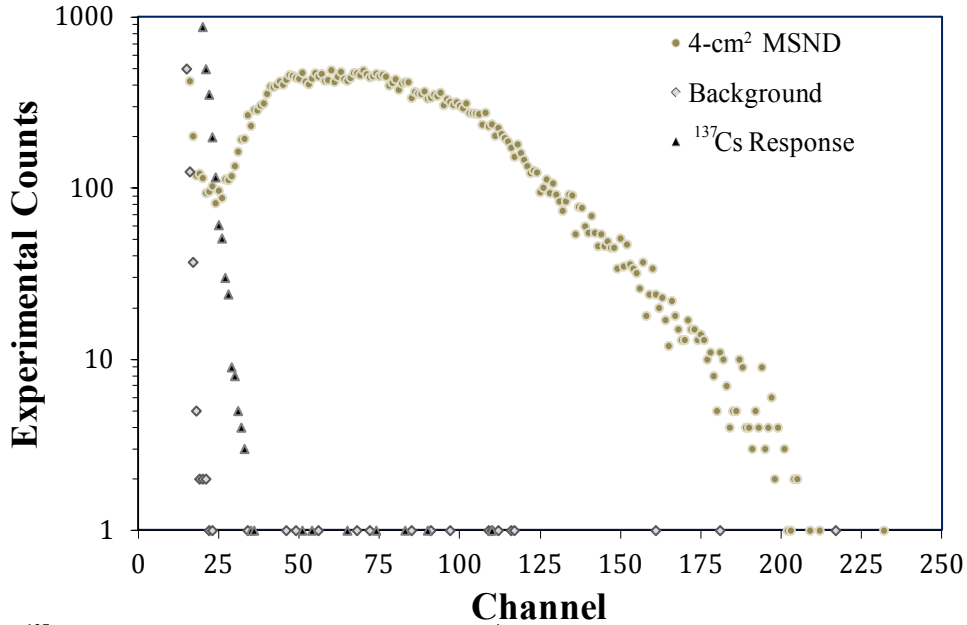


**Fig. 7.** Measured  $^{137}\text{Cs}$  gamma-ray irradiation ( $\Omega_F = 1.27 \times 10^{-4}$ ) and neutron irradiation pulse-height spectral features for the individual 4-cm<sup>2</sup> MSND with the 10- $\mu\text{s}$  signal integration time design.

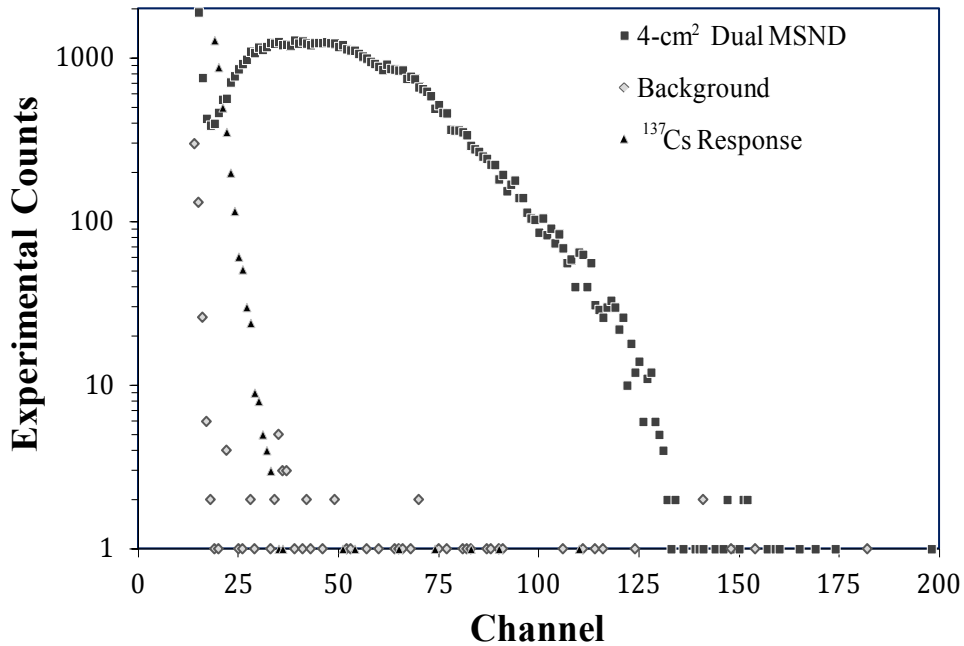


**Fig. 8.** Measured  $^{137}\text{Cs}$  gamma-ray irradiation ( $\Omega_F = 1.27 \times 10^{-4}$ ) and neutron irradiation pulse-height spectral features for the stacked 4-cm<sup>2</sup> MSND with the 10- $\mu\text{s}$  signal integration time design.

The gamma-ray pulse-height spectrum response for the stacked 4-cm<sup>2</sup> large-area MSND is shown in Fig. 8. With the LLD set at channel 18, the gamma-ray detection efficiency was determined to be approximately  $5.44 \times 10^{-5}$  measured-event per gamma ray and with the LLD set to channel 28, the gamma-ray detection efficiency is approximately  $7.90 \times 10^{-8}$  measured-event per gamma ray. The  $n/\gamma$  response for 662 keV photons is then easily calculated by dividing the MSND detection efficiency by the gamma-ray detection efficiency. From Fig. 9, the  $n/\gamma$  ratio for the stacked MSNDs with an LLD set at channel 18 is  $5.95 \times 10^3$  and with an LLD set at channel 28 is  $3.67 \times 10^6$ .

These data are summarized in Table 1. Stacked MSNDs show a downward energy shift in the pulse-height distribution to that of an individual MSND, which can decrease the  $n/\gamma$  rejection ratio. In addition, the stacked MSND has more bulk silicon, because there are two MSND chips that can interact with gamma rays, thereby, decreasing the  $n/\gamma$  rejection ratio. Again, the MSND gamma-ray response measurement was performed in the KSU nuclear reactor bay, which has a higher background of albedo neutrons than natural background.

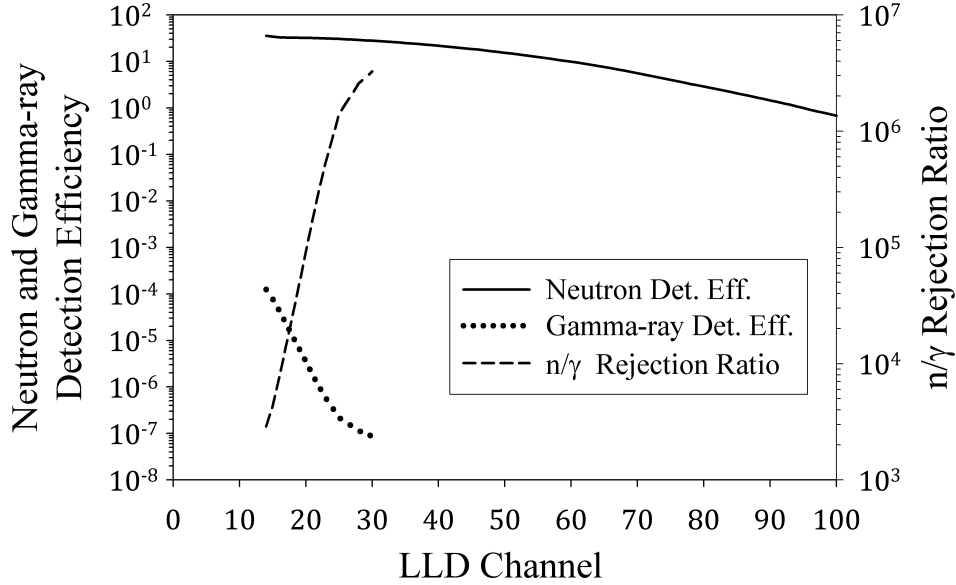


**Fig. 9.** Comparison of the measured neutron detection efficiency, the measured  $^{137}\text{Cs}$  gamma-ray detection efficiency, and the  $n/\gamma$  rejection ratio of the stacked 4-cm<sup>2</sup> MSND.

Notice in Table 1 that, for the stacked 4-cm<sup>2</sup> MSNDs with the LLD set in the pulse-height distribution dip, the neutron detection efficiency is high and nearly double that of the individual MSND, but the  $n/\gamma$  rejection ratio is very poor. However, when the LLD is raised to channel 28, with a neutron detection efficiency loss of three percentage points, the  $n/\gamma$  rejection ratio is very high. Again this demonstrates the advantage of the  $^6\text{Li}$  high-energy neutron reaction products over that of neutron reaction products from  $^{10}\text{B}$  (compare [3, 13]) and neutron reaction products from  $^{157}\text{Gd}$  for gamma-ray discrimination, without detriment to the neutron detection efficiency.

**Table 1.** Individual and stacked 4-cm<sup>2</sup> MSND thermal-neutron ( $\epsilon_{\text{th}}$ ) and  $^{137}\text{Cs}$  gamma-ray ( $\epsilon_{\gamma}$ ) detection efficiencies and neutron to gamma-ray rejection ratio ( $n/\gamma$ ) for a specified LLD.

LLD (Chn)	$\epsilon_{\text{th}}$	$\epsilon_{\gamma}$	$n/\gamma$
<u>Individual MSND</u>			
25	16.3%	$1.85 \times 10^{-4}\%$	$8.83 \times 10^4$
32	15.9%	$3.95 \times 10^{-6}\%$	$4.04 \times 10^6$
<u>Stacked MSND</u>			
18	32.4%	$5.44 \times 10^{-3}\%$	$5.95 \times 10^3$
28	29.0%	$7.90 \times 10^{-6}\%$	$3.67 \times 10^6$



### 3.4 Discussion

The measured 32% thermal-neutron detection efficiency for the 200- $\mu\text{m}$  deep etched MSND was not as high as the 40% thermal neutron detection efficiency predicted by a model developed elsewhere [2, 3]. This discrepancy can be explained as follows. First, the bottom stacked device trench alignment may not have been well aligned with the top detector. This has two consequences: neutron streaming can occur for areas not intersected by the converter and the top detector absorber may be shadowing the bottom detector absorber. Overall, the result is a decrease in detection efficiency. Second, the shift may be due to charge collection losses and a ballistic deficit studied elsewhere [1, 14]. Future work will be dedicated to better construction, aligning and bonding methods. Also, new fabrication designs of interlaced microstructures, that are etched from both sides of the Si diode, shown elsewhere [11, 15], are being employed. The fabrication design will improve the electric-field strength, making it uniformly distributed across the Si detector volume so as to reduce the signal integration time.

## 4. CONCLUSION

Based on the results and observations presented here, the following can be stated:

1. Higher efficiency with large-area MSNDs can be achieved by stacking the semiconductor detectors. The efficiencies for symmetric trench devices can be doubled by capturing streaming neutrons from the first detector.
2. With low LLD settings and minimal feature sizes, an individual MSND with asymmetric features (trenches wider than semiconductor fins) offers high efficiencies. However, with the LLD set at channels generally necessary to discriminate against background gamma rays, the stacked trench design with symmetric features outperforms the asymmetric designs (stacked or not).
3. A dual-integrated, 4- $\text{cm}^2$  straight-trench microstructured Si detector, backfilled with  $^6\text{LiF}$  powder has been characterized for neutron sensitivity in a diffracted 0.0253 eV thermal-neutron beam from a TRIGA Mark II nuclear reactor. An important advantage for the dual-integrated stacked MSND design is the high efficiency achieved by appropriately stacking two detector chips into a single device. The dual-integrated stacked MSND with two 200- $\mu\text{m}$  deep trenched devices achieved 32% intrinsic efficiency.

Stacked MSNDs, backfilled with  $^6\text{LiF}$ , offer high thermal-neutron detection efficiency in a compact package. Variants on the microstructure design have been reported, which include sinusoidal trenches, chevron trenches, circular hole, pillar [3, 5].

## ACKNOWLEDGEMENTS

This work was supported under DTRA contract DTRA01-02-D-0067.

## REFERENCES

- [1] S. L. Bellinger, W. J. McNeil, and D. S. McGregor, "Improved Fabrication Technique for Microstructured Solid-State Neutron Detectors." 1164, 57-65.
- [2] S. L. Bellinger, R. G. Fronk, W. J. McNeil *et al.*, "Characteristics of the Stacked Microstructured Solid-State Neutron Detector." 7805, 78050-16.
- [3] J. K. Shultis, and D. S. McGregor, "Design and Performance Considerations for Perforated Semiconductor Thermal-Neutron Detectors," Nucl. Instrum. and Meth., A606, 608-636 (2009).
- [4] NIST Center for Neutron Research, <http://www.ncnr.nist.gov/resources/n-lengths/elements/si.html>, [June, 2010].
- [5] C. J. Solomon, J. K. Shultis, and D. S. McGregor, "Reduced Efficiency Variation in Perforated Neutron Detectors with Sinusoidal Trench Design," Nucl. Instrum. and Meth., A618, 260-265 (2010).
- [6] J. Dingley, Y. Danon, N. LiCausi *et al.*, "Directional Response of Microstructure Solid State Thermal Neutron Detectors," Transactions of the American Nuclear Society and Embedded Topical Meeting Isotopes for Medicine and Industry, 103, 1190-1191 (2010).

- [7] B. B. Rice, [Inductively Coupled Plasma Etching of Silicon and Gallium Arsenide] Kansas State University, Manhattan, KS(2006).
- [8] D. S. McGregor, W. J. McNeil, S. L. Bellinger *et al.*, "Microstructured Semiconductor Neutron Detectors," Nucl. Instrum. and Meth., A608, 125-131 (2009).
- [9] D. S. McGregor, and J. K. Shultis, "Reporting Detection Efficiency for Semiconductor Neutron Detectors: A Need for a Standard," Nucl. Instrum. and Meth., A632(1), 167-174 (2011).
- [10] T. C. Unruh, "Development of a neutron diffraction system and neutron imaging system for beamport characterization," M.S. Thesis, Kansas State University, Manhattan, KS, 2009.
- [11] S. L. Bellinger, R. G. Fronk, T. J. Sobering *et al.*, "Improved High Efficiency Stacked Microstructured Neutron Detectors Backfilled with Nanoparticle  $^6\text{LiF}$ ," IEEE Trans. Nucl. Sci., 59(1), 167-173 (2012).
- [12] M. S. Gordon, P. Goldhagen, K. P. Rodbell *et al.*, "Measurement of the flux and energy spectrum of cosmic-ray induced neutrons on the ground," IEEE Trans. Nucl. Sci., 51(6), 3427-3434 (2004).
- [13] R. J. Nikolic, A. M. Conway, C. E. Reinhardt *et al.*, "6:1 Aspect Ratio Silicon Pillar Based Thermal Neutron Detector Filled with  $^{10}\text{B}$ ," Appl. Phys. Lett., 93(13), 133502-5 (2008).
- [14] W. J. McNeil, "Perforated Diode Neutron Sensors," Ph.D. Dissertation, Kansas State University, Manhattan, KS, 2010.
- [15] D. S. McGregor, and R. T. Klann, *High-Efficiency Neutron Detectors and Methods of Making the Same*, Patent, U.S.P.T.O., US-7164138, January 16, 2007.